

# Wavelet analysis of soil-structure interaction effects on seismic responses of base-isolated nuclear power plants

Shafayat Bin Ali\*<sup>1</sup> and Dookie Kim<sup>2a</sup>

<sup>1</sup>Institute of Earthquake Engineering Research (IEER), Chittagong University of Engineering & Technology, Chittagong-4349, Bangladesh  
<sup>2</sup>Department of Civil and Environmental Engineering, Kunsan National University, South Korea

(Received July 21, 2016, Revised January 10, 2018, Accepted January 16, 2018)

**Abstract.** Seismic base isolation has been accepted as one of the most popular design procedures to protect important structures against earthquakes. However, due to lack of information and experimental data the application of base isolation is quite limited to nuclear power plant (NPP) industry. Moreover, the effects of inelastic behavior of soil beneath base-isolated NPP have raised questions to the effectiveness of isolation device. This study applies the wavelet analysis to investigate the effects of soil-structure interaction (SSI) on the seismic response of a base-isolated NPP structure. To evaluate the SSI effects, the NPP structure is modelled as a lumped mass stick model and combined with a soil model using the concept of cone models. The lead rubber bearing (LRB) base isolator is used to adopt the base isolation system. The shear wave velocity of soil is varied to reflect the real rock site conditions of structure. The comparison between seismic performance of isolated structure and non-isolated structure has drawn. The results show that the wavelet analysis proves to be an efficient tool to evaluate the SSI effects on the seismic response of base-isolated structure and the seismic performance of base-isolated NPP is not sensitive to the effects in this case.

**Keywords:** nuclear power plant; base isolation; seismic behavior; soil-structure interaction; wavelet analysis

## 1. Introduction

The dynamic behavior of inelastic structures during seismic excitation is a complex non-stationary process. The conventional Fourier analysis allows to decompose a non-stationary signal to complex exponential functions as a superposition of series of sine and cosine to obtain the frequency content of the signal in the time domain. The main disadvantage of Fourier analysis is that it cannot provide any time located information of these frequencies. In contrast, wavelet analysis is a powerful tool which provides both time and frequency localized information of a signal simultaneously. The wavelet analysis was first applied in the development of oil and gas field (Goupillaud *et al.* 1984). Subsequently, many researchers have developed the methodology of wavelet analysis (Daubechies 1992 and Meyer 1992). Wavelet tool was used by Newland (1994) for analysing vibration records and developing special wavelets for engineering purposes. However, wavelet analysis has been used in damage detection of structural element and structural health monitoring (Melhem and Kim 2003 and Yi *et al.* 2013). In recent times, wavelets have been applied in seismic engineering to investigate acceleration responses of dynamic systems (Iyama and Kuwamura 1999 and Chatterjee and Basu 2004).

Seismic base isolation has been considered as a prominent technique to protect structures against seismically induced ground motions. Many studies were conducted to investigate the efficiency of base isolation system under seismic excitation (Stewart *et al.* 1999, Kani *et al.* 2006). Recently, seismic base isolation has been applied in design and construction of different kind of structures such as, conventional buildings, bridges, and NPP industry. Up to date, only six nuclear reactors in two nuclear power plants (NPPs) in France and South Africa have been constructed with seismic base isolation system (Malushte and Wittaker 2005, Huang *et al.* 2010). Additionally, a new nuclear reactor in France is under construction with seismic base isolation devices (Forni 2011). Furthermore, many researchers have investigated the seismic responses of base-isolated NPP structures under seismic loading (Micheli *et al.* 2004, Zhao and Chen 2013). Though, Forni *et al.* (2012) have provided rough recommendations on the design and construction of base isolation system of NPP, however, till now there is no specific standards for base isolated NPPs.

Since the inelastic behavior of soil beneath a structure may play an important role to alter the seismic response of the superstructure, the consideration of soil-structure interaction (SSI) on the seismic analysis and design is essential. The common practice usually ignores the SSI effects on seismic response of base isolated infrastructure. Recently many studies have been focused on the significance to consider the effects of SSI on design of important infrastructures. The SSI effects on the modal properties of base-isolated buildings were investigated by Novak and Henderson (1989) and concluded that the effect should not be ignored for the isolated structures.

\*Corresponding author, Research Lecturer

E-mail: shafayat@cuet.ac.bd

<sup>a</sup>Professor

E-mail: kim2kie@kunsan.ac.kr

Tongaonkar and Jangid (2003) numerically evaluated the effect of SSI on a three-span bridge and led to the conclusion that SSI has incremental effect in seismic displacements of bridges. Spyrakos *et al.* (2009) investigated the SSI effect on the response of base-isolated buildings and the conclusion was that the SSI has significant effect on modal properties of squat and stiff base-isolated structures. Mahmoud *et al.* (2012) conducted a parametric study to compare the responses of isolated structure with and without SSI under different ground motions and found that SSI has slight influence on the response of flexible structures. Sharmin *et al.* (2017) investigated the influence of SSI on seismic responses of offshore wind turbine with considering earthquake incident angle.

The ambiguous conclusions of the above studies indicate that additional research is needed to evaluate the effects of SSI on the seismic performance of isolated structures. The present study focuses on the investigation of SSI effects on seismically isolated nuclear power plant structures. A time frequency tool based on wavelet analysis is used to evaluate the time frequency characteristics of ground motion and acceleration response of the structures. A comparison between seismic performance of isolated and non-isolated NPP has drawn to show the effectiveness of the isolation system. Furthermore, the correlation between wavelet coefficients of input ground motion and acceleration response of structure has been evaluated to identify the short-term changes in the frequency content of the response.

## 2. Nuclear Power Plant (NPP) structure

### 2.1 NPP stick model

The Korean standard nuclear reactor APR1000 (Advanced Power Reactor) is adopted for numerical analysis. The APR1000 is a pressurized water reactor (PWR), and Fig. 1 demonstrates its lumped mass stick model beside the hypothetical structural diagram of NPP containment building (Lee and Song 1999).

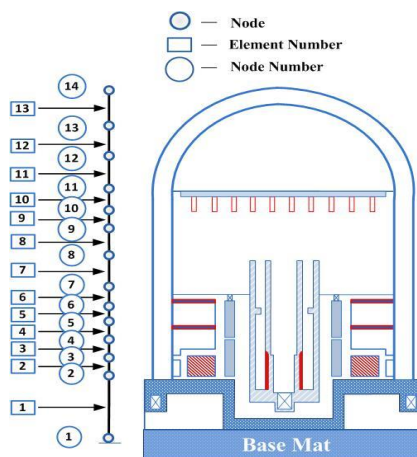


Fig. 1 NPP stick model and sectional elevation of containment building

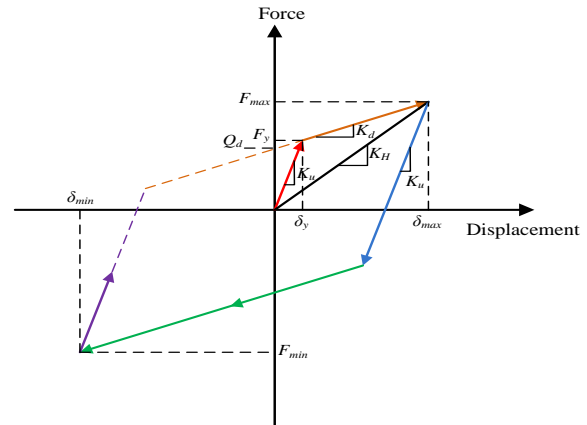


Fig. 2 Linearization of the force-displacement relationship of LRB isolator

The total height of the model is 65.8m. The stick model of the NPP consists of fourteen nodes and thirteen three dimensional beam elements. The actual translational and rotational masses of the NPP are also transferred to the corresponding nodes on each element's edge as lumped masses.

### 2.2 Design of base isolator

The lead rubber bearing (LRB) isolation device is used to provide discontinuity between foundation and the NPP structure. The LRB isolation device consists of low damping natural rubber, steel plates and a lead plug damper. The alternating laminations of thin rubber layers and steel plates bonded together to provide horizontal flexibility and vertical rigidity, and the lead plug is used to add damping to the isolation system. In this study, the design of LRB isolator is adopted from the international Organization for Standardization (ISO) specification (2010). The present study considered equivalent linear properties of the isolation device, demonstrated in Fig. 2. In Fig. 2,  $K_u$  denotes the linear (unloading) horizontal tangential stiffness.  $K_d$  and  $K_H$  are the post-yield horizontal stiffness and the effective horizontal stiffness of the isolator respectively.  $Q_d$  and  $F_y$  represent the characteristic strength and the yield strength respectively.  $\delta_{max}$  and  $\delta_{min}$  denote the maximum horizontal displacement and the minimum horizontal displacement of the isolator, respectively. And  $F_{max}$  and  $F_{min}$  represent the maximum and the minimum horizontal forces corresponding to the maximum and the minimum displacements of the isolator, respectively.

In this study, the total weight of base-isolated NPP structure is 110,950 tons, which is used for calculating and designing the dynamic properties of the LRB isolators. The following equation represents the horizontal stiffness of the isolators, after the yielding of the lead damper

$$K_{total} = M \left( \frac{2\pi}{T_H} \right)^2 \tag{1}$$

where  $K_{total}$  represents the total global horizontal tangential stiffness of the system. In addition,  $M$  denotes the total mass of the NPP structure with base mat and  $T_H$  denotes the

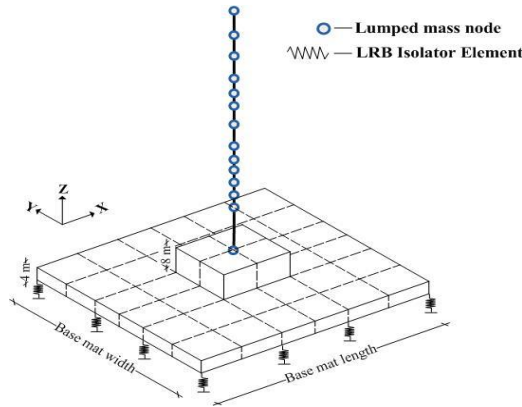


Fig. 3 Nuclear island base mat dimensions

Table 1 Properties of the LRB base isolator

Horizontal Stiffness	Post-yielding Stiffness	Yield Strength	Characteristic Strength	Yield Displacement	Hardening ratio
$K_H$ (kN/m)	$K_d$ (kN/m)	$F_y$ (kN)	$Q_d$ (kN)	$\delta_y$ (mm)	$\alpha$
8436.10	7089.55	303.73	269.31	4.85	0.113

target fundamental period of NPP structure, which is considered as 2 sec preliminarily. The calculation of horizontal stiffness of single isolator of base-isolated NPP is denoted by the following equation

$$K_H = \frac{K_{total}}{N} \quad (2)$$

In the above equation,  $K_H$  represents the horizontal (effective) tangential stiffness of the single isolator.  $N$  is number of isolators. In this study, 121 LRB isolators are used for base isolation system. Before the yielding of the lead plug the linear (unloading) horizontal stiffness of the isolator can be expressed as  $K_u=(4\sim 6.5)\times K_H$ , while the yield strength can be represented as  $F_y=(0.03\sim 0.05)\times W$ , where  $W$  is the total weight of NPP. In this study,  $K_u$  and  $F_y$  are considered as  $4K_H$  and  $0.05W$  respectively. Furthermore, the characteristic strength of the isolator is represented as

$$Q_d = F_y \left(1 - \frac{K_H}{K_u}\right) \quad (3)$$

And the hardening ratio of isolator can be expressed as

$$\alpha = \frac{K_d}{K_u} \quad (4)$$

Tables 1 and 2 illustrate the dynamic properties and dimensions of LRB isolator for the base-isolated nuclear power plant structure.

Table 2 Dimensions of the component of LRB base isolator

No. of rubber layers	Rubber layer thickness (mm)	Total thickness of rubber layers (mm)	Total thickness of isolator (mm)	Lead plug diameter (mm)	Outer diameter of isolator (mm)
10	18	180	350	210	1950

Table 3 Base mat dimensions of BI-NPP model

Base mat dimensions		No. of LRB isolators		Total no. of isolators	
Length (m)	Width (m)	Area (m <sup>2</sup> )	along X-dir.		along Y-dir.
100	80	8000	11	11	121

### 2.3 Base mat of nuclear island

The structural model of base-isolated nuclear power plant is established with the stick model of NPP containment building and the base mat with 121 LRB isolators. The total thickness of the base mat under the NPP stick model is 12 m, with dimensions (20 m × 16 m), and the thickness is 4 m for the rest of the base mat area. The total modeling is done by OpenSees Navigator, compatible with OpenSees platform (Schellenberg *et al.* 2013). Table 3 represents the base mat dimensions and number of isolators in each direction of BI-NPP model. Fig. 3 demonstrates the base mat dimensions in the global axes.

## 3. Ground motion characteristics

To examine the seismic behavior of the nuclear power plant structure three large and well recorded earthquakes are selected i.e., 1940 El Centro, 1989 Loma Prieta, and 1995 Kobe. The Fig. 4(a), (c) and (e) represent the acceleration time history of El Centro, Loma Prieta and Kobe record with a time increment of 0.02 sec, 0.005 sec and 0.01 sec respectively. The peak ground acceleration (PGA) of the ground motions are 0.32g, 0.32g and 0.69g respectively.

The first 31.36 sec, 39.95 sec and 40.95 sec of these records are used for time history analysis. The Fig. 4(b), (d) and (f) show the Fourier based power spectral density (PSD) of these excitations. It is observed from the Figs. that the predominant frequency of the records are 1.51 Hz, 0.37 Hz and 2.12 Hz respectively. Table 4 represents the information of selected earthquake ground motions.

## 4. Wavelet analysis

A wavelet is a small localized wave that starts with zero

Table 4 Characteristics of selected ground motions

No.	Earthquake	Year	Magnitude Mw	Source Mechanism	Duration (sec)	PGA (g)	PGV (m/s)	Predominant frequency (Hz)
1	El Centro	1940	7.0	Strike-Slip	31.36	0.32	0.33	1.51
2	Loma Prieta	1989	6.9	Oblique	39.95	0.32	0.43	0.37
3	Kobe	1995	6.9	Strike-Slip	40.95	0.69	0.85	2.12

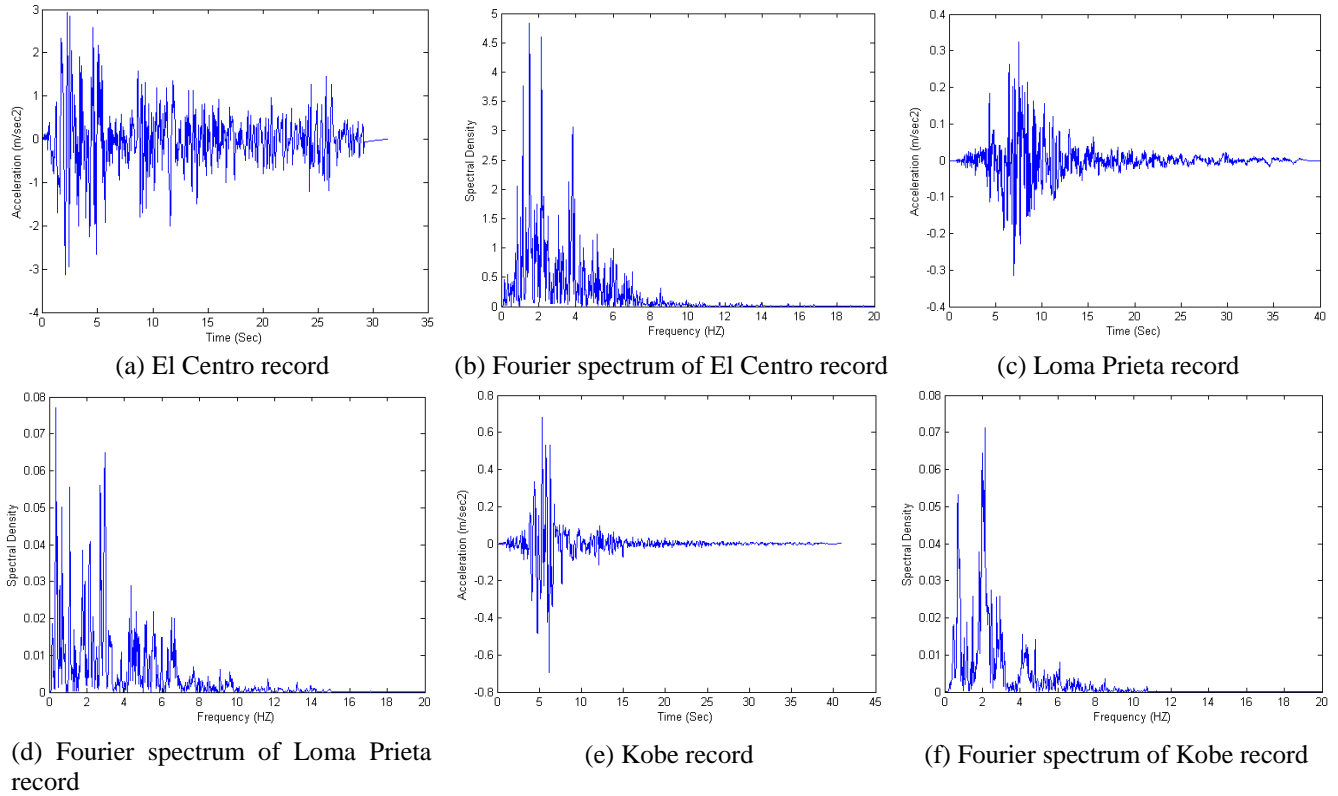


Fig. 4 Acceleration time history and Fourier based power spectral density (PSD) of selected ground motions

and back to zero after a few oscillations. The wavelet is used as a basis function to analysis the transient, non-stationary signals with sharp discontinuities (Sarica and Rahman 2003). The wavelet transform has most attractive feature to represent the energy components over different frequency contents of the signals, which is unavailable in the Fourier transform (Iyama and Kuwamura 1999). The wavelet transforms are mainly two types; the continuous wavelet transforms and the discrete wavelet transform. The main advantage of the discrete wavelet transform is that no redundant components are existed in transferred data and the inverse transform is possible to any time-frequency data. In this study, the discrete wavelet transform is applied and referred as “wavelet transform” for simplicity.

#### 4.1 Wavelet decomposition

The acceleration signal is divided into two signals called, the approximations and the details, by passing through two complementary filters: i.e., a low-pass filter and a high-pass filter. The portions of the original signal which passed through low-pass filter are the high-scale and content low frequency component. They are denoted as the “approximations”. And high-pass portions of the signal which called the “details” are the low-scale and content high-frequency component. The decomposition process of the signal is shown in Fig. 5. This process is denoted by the following equation

$$S_j(t) = a_{j+1}(t) + d_{j+1}(t) \quad (5)$$

where  $S(t)$  represents the original signal,  $a(t)$  is the

Table 5 Frequency and time range of each decomposition level of El Centro record

Decomposition level	Frequency (Hz)	Time interval (sec)
1	12.5-25	0.08-0.04
2	6.25-12.5	0.16-0.08
3	3.125-6.25	0.32-0.16
4	1.562-3.125	0.64-0.32
5	0.781-1.562	1.28-0.64
6	0.3905-0.781	2.56-1.28
7	0.195-0.3905	5.13-2.56

Table 6 Frequency and time range of each decomposition level of Loma Prieta record

Decomposition level	Frequency (Hz)	Time interval (sec)
1	50-100	0.02-0.01
2	25-50	0.04-0.02
3	12.5-25	0.08-0.04
4	6.25-12.5	0.16-0.08
5	3.125-6.25	0.32-0.16
6	1.562-3.125	0.64-0.32
7	0.781-1.562	1.28-0.64
8	0.3905-0.781	2.56-1.28
9	0.195-0.3905	5.13-2.56
10	0.0975-0.195	10.26-5.13

approximations component, and  $d(t)$  is the details component. And  $j$  denotes the level number of the particular range of frequency content of the signal.

The Eq. (6) is expressed the range of frequency content

Table 7 Frequency and time range of each decomposition level of Kobe record

Decomposition level	Frequency (Hz)	Time interval (sec)
1	25-50	0.04-0.02
2	12.5-25	0.08-0.04
3	6.25-12.5	0.16-0.08
4	3.125-6.25	0.32-0.16
5	1.562-3.125	0.64-0.32
6	0.781-1.562	1.28-0.64
7	0.3905-0.781	2.56-1.28
8	0.195-0.3905	5.13-2.56
9	0.0975-0.195	10.26-5.13

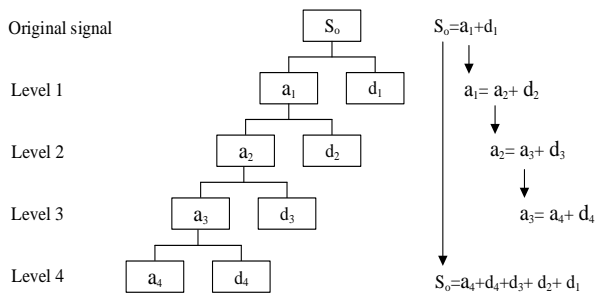


Fig. 5 Decomposition levels

where  $\Delta t$  represents the time step of the acceleration signal.

$$\omega_j = [\omega_{1j}, \omega_{2j}]$$

where 
$$\omega_{1j} = \frac{1}{2^{j+1} \Delta t}, \omega_{2j} = \frac{1}{2^j \Delta t} \tag{6}$$

The frequency ranges of decomposition levels of El Centro, Loma Prieta, and Kobe records are presented in Tables 5-7. According to Fig. 5 the original signal can be expressed as follows

$$S_o(t) = a_n(t) + \sum_{j=1}^n d_j(t) \tag{7}$$

where  $n$  is the total number of decomposition levels. The decomposition of a signal should be done at a level where there is no valuable information is contained by the approximation. Without any loss of information the original signal can be represented from details as follows (Sarica and Rahman 2003)

$$S_o(t) = \sum_{j=1}^n d_j(t) \tag{8}$$

The details components of the original signal can be expressed as

$$d_j(t) = \sum_{-\infty}^{\infty} c_{j,k} \psi_{j,k} \tag{9}$$

In the above,  $k$  is an index of time scale,  $c_{j,k}$  represent the corresponding wavelet coefficients, and  $\psi_{j,k}$  are the basis wavelet functions, which are denoted as

$$\psi_{j,k} = 2^{\frac{j}{2}} \psi(2^j t - k) \tag{10}$$

Thus finally, the original signal with time interval  $[0, t]$  can be rewritten as

$$S_o(t) = \sum_{j=1}^n \sum_{k=0}^t c_{j,k} \psi_{j,k} \tag{11}$$

In this study, the 4th order Daubechies (db4) mother wavelet is used as a basis wavelet function which is suitable for the general case of earthquake excitation analysis (Li *et al.* 2009). Fig. 6 shows the 4th order Daubechies mother wavelet.

The wavelet analysis starts with the decomposition procedure of the applied ground motions and acceleration responses of structures to evaluate the wavelet coefficients and the wavelet functions at different levels. As an example,

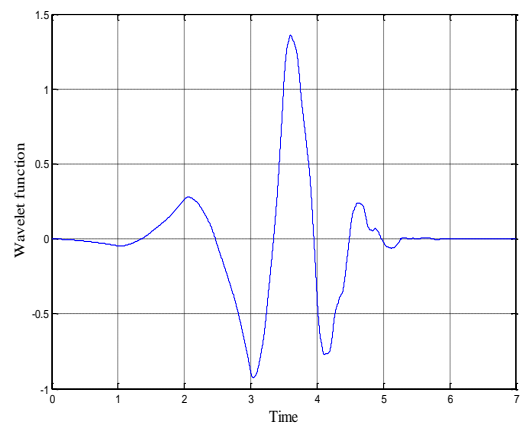
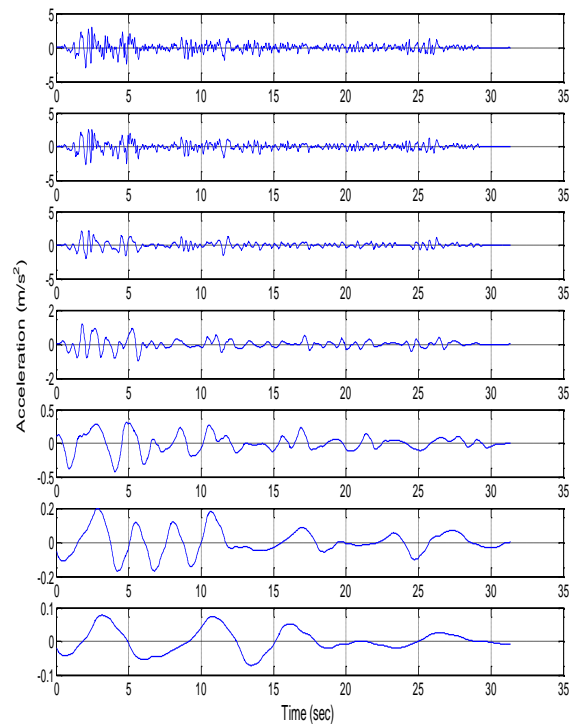
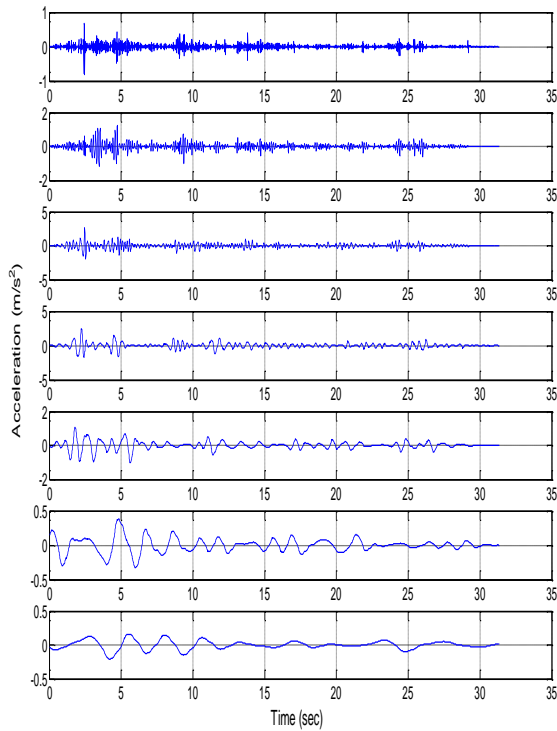


Fig. 6 Daubechies basis function (db4)



(a) Approximations

Fig. 7 Approximation and detail functions of seven decomposition levels of El Centro record



(b) Details

Fig. 7 Continued

the approximation and detail functions of seven decomposition levels of El Centro record from level 1 to level 7 are presented from the top to the bottom in Fig. 7.

#### 4.2 Energy calculation using wavelet transform

According to Walker (1999), the total energy of a discrete signal is the sum of the squares of its values and is expressed as

$$E = \Delta t \sum_{t=0}^t S_o^2(t) \tag{12}$$

where  $\Delta t$  denotes the sampling period. The above definition is similar to Arias intensity measure. The Arias intensity of  $S_o(t)$  is defined as (Kayen and Mitchell 1997)

$$E = \frac{\pi}{2g} \int_0^t S_o^2(t) dt \tag{13}$$

In the above equation,  $g$  denotes the earth's gravity. Sarica and Rahman (2003) illustrated that the total energy of a signal can be represented as the sum of the squares of details only at each decomposition level. In this study, this concept is used to evaluate the total energy of acceleration signal which is expressed as

$$E = \sum_{j=1}^n \sum_{k=0}^t d_j^2(t) \tag{14}$$

### 5. Soil structure interaction

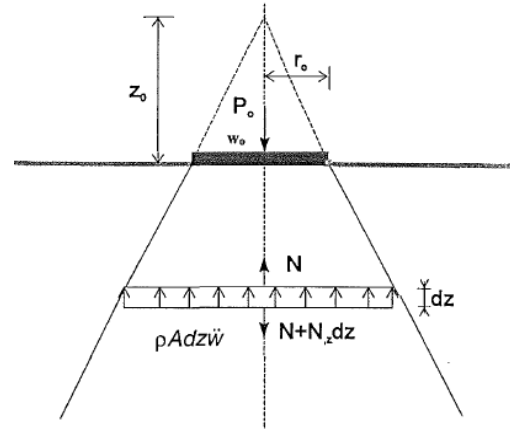


Fig. 8 Cone model for translational modes of vibration (Wong *et al.* 1977)

In the present study SSI system is adopted by using sub-structure methodology where the structure and the soil stratum are modelled separately and then combined together to constitute a soil-structure model. The underlying soil of the structure is assumed as a homogeneous half-space and substitute with a simplified model based on the concept of cone model, developed by Meek and Wolf (1993) and Wolf (1994). In this model a truncated semi-infinite cone is used to obtain soil-structure interaction mechanism. The model is based on the assumption that the superstructure is rested on a homogenous semi-infinite soil layer to extract soil springs and dashpots (Ahmadi 2015).

In semi-infinite truncated cone the stress distribution area under the structure is considered increases linearly with depth which is shown in Fig. 8.

$$A = \left( \frac{z}{z_0} \right)^2 A_0 \tag{15}$$

where  $A$  represents the stress distribution area at any depth  $z$  of the cone and  $A_0$  (equals to  $\pi r_0^2$ ) represents the equivalent disk area on the surface. For translational modes of vibration the radius of equivalent disk is obtained by equating the area of the rectangular foundation to that of an equivalent disk.

To derive dynamic stiffness coefficient for translational modes of vibration an element of semi-infinite truncated cone is considered with infinitesimal height  $dz$  and cross-sectional area  $z$ . An axial force  $N$  is subjected to the element which is resulting from a vertical force  $P_o$  acting on the disk. The axial displacement from the apex of the cone of the disk is  $w_o$  and  $w$  at any depth  $z$  resulting from  $P_o$ . The static equilibrium condition at the element is expressed as

$$-N + N + \frac{\partial N}{\partial z} dz = 0 \tag{16}$$

The expression can be written when the element is subjected to a harmonic force

$$-N + N + \frac{\partial N}{\partial z} dz - \rho A \ddot{w} dz = 0 \tag{17}$$

From the force-displacement and constitutive

relationships following expression is obtained

$$N = E_c A \frac{\partial w}{\partial z} \quad (18)$$

In the above equation,  $E_c$  represents the constrained modulus which is defined as  $\rho v_p^2$  or  $(2G_s)(1-\nu)/(1-2\nu)$ .  $\rho$  denotes the mass density ( $\text{kg/m}^3$ ),  $G_s$  denotes the elastic shear modulus ( $\text{N/mm}^2$ ),  $v_p$  denotes the dilatational wave velocity (m/s) and  $\nu$  denotes Poisson's ratio of the soil.

The wave propagation Eq. (19) is obtained by substituting Eq. (18) into Eq. (17).

$$\frac{\partial^2}{\partial z^2}(zw) - \frac{1}{v_p^2} \frac{\partial^2}{\partial t^2}(zw) = 0 \quad (19)$$

Considering outwardly propagating waves only, the solution of above equation is

$$zw = z_0 f\left(t - \frac{z - z_0}{v_p}\right) \quad (20)$$

where  $f$  is an arbitrary function. When  $w = w_0$  at  $z = z_0$  the  $f(t) = w_0$  so the expression is

$$w = \frac{z_0}{z} w_0 \left(t - \frac{z - z_0}{v_p}\right) \quad (21)$$

The first derivative of the above equation with respect to  $z$  is

$$\frac{\partial w}{\partial z} = -\frac{z_0}{z^2} w_0 \left(t - \frac{z - z_0}{v_p}\right) - \frac{z_0}{z v_p} w_0' \left(t - \frac{z - z_0}{v_p}\right) \quad (22)$$

where  $w_0'$  represents the first derivative of  $w_0$  with respect to the argument  $[t - (z - z_0)/v_p]$ . Applying Eq. (22) into Eq. (18) at  $z = z_0$  leads to

$$P_0 = -N(z = z_0) = \frac{\rho v_p^2 A_0}{z_0} w_0 + \rho v_p A_0 \hat{w}_0 \quad (23)$$

where  $\hat{w} = w_0' \{t - (z - z_0)/v_p\}$  at  $z = z_0$ . The above equation is the force displacement relationship for vertical vibration which represents both components of translational motion, i.e., vertical and horizontal components as follows

$$P_0 = \frac{\rho v^2 A_0}{z_0} w_0 + \rho v A_0 \hat{w}_0 \quad (24)$$

$$\text{or} \quad P_0 = k w_0 + c \hat{w}_0 \quad (25)$$

$$\text{with} \quad k = \frac{\rho v^2 A_0}{z_0} \quad (26)$$

$$\text{and} \quad c = \rho v A_0 \quad (27)$$

where  $k$  and  $c$  represent the frequency independent stiffness and viscous damping coefficient respectively (Ghaffar-Zade and Cahpel 1983). And  $v$  is the dilatational wave velocity for vertical motion and shear wave velocity for horizontal motion.

For rotational modes of vibration the radius of equivalent disk is obtained by equating moment of inertia of

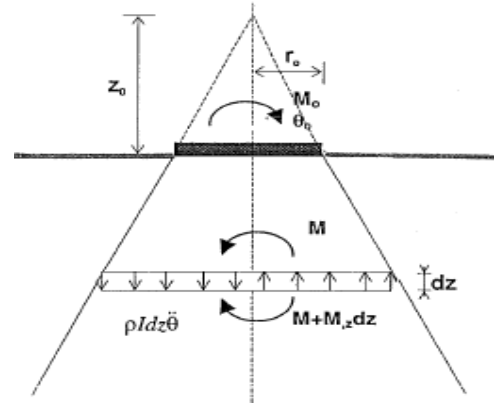


Fig. 9 Cone model beneath rigid foundation for rotational degree-of-freedom (Wong *et al.* 1977)

the rectangular foundation to the moment of inertia (rocking) or polar moment of inertia (torsion) of an equivalent disk. Fig. 9 represents the cone model associated with rotational degree of freedom where  $M$  is the moment subjected to the equivalent disk,  $\theta$  is the angle of rotation of the disk due to the moment and  $I_0$  is the moment of inertia of disk about the axes of rotation.

The coefficient of the spring and dashpot for rotational modes of vibration are as follows

$$k_\theta = \frac{3\rho v^2 I_0}{z_0} \quad (28)$$

$$c_\theta = \rho v I_0 \quad (29)$$

where  $v$  is the dilatational wave velocity for rocking mode and shear wave velocity for torsional mode.

In order to consider soil material damping a vigot viscoelastic model is used. In this model each original spring is augmented by a dashpot in parallel and each original dashpot is augmented by a pulley mass without changing masses in the original model (Wolf 1994). The coefficients of dashpot and pulley mass for translational and rotational modes of vibration are expressed by Eqs. 30 and 31 respectively.

$$c' = 2 \frac{\zeta_0}{\omega_0} k, \quad m' = \frac{\zeta_0}{\omega_0} c \quad (30)$$

$$c'_\phi = 2 \frac{\zeta_0}{\omega_0} k_\phi, \quad m'_\phi = \frac{\zeta_0}{\omega_0} c_\phi \quad (31)$$

where  $\zeta_0$  is the soil's damping ratio and  $\omega_0$  is the fundamental frequency of the soil-structure system.

In this study, total five degrees of freedoms are considered in the cone model by allowing sway and rocking motions about  $x$  and  $y$  directions and torsion about  $z$  direction. Two soil types are considered in the SSI model i.e., soft rock (shear wave velocity  $V_s = 600$  m/s) and rock (shear wave velocity  $V_s = 1000$  m/s) for reflecting the real site conditions of NPP structures. The other soil parameters used in this study are:  $\rho = 2100$   $\text{kg/m}^3$  (density of soil),  $\nu = 0.4$  (Poisson's ratio) and  $\zeta_0 = 0.05$ . Fig. 10 shows the soil model used in this study.

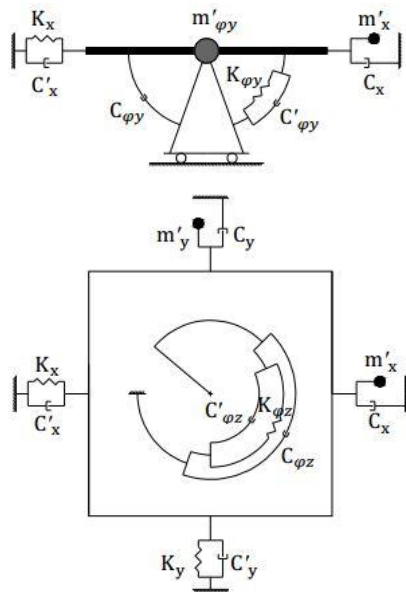


Fig. 10 Soil model (Kenarangi and Rofooei 2010)

## 6. Results and discussions

Two analysis conditions are considered of the nuclear power plant model i.e., without adopting the base-isolation system, which is simply denoted by “NPP” and with adopting the base-isolation system, which is denoted by “BI-NPP”. To incorporate the SSI effect to the structure, a discrete cone model is considered. Two shear wave velocities are used to consider soft rock ( $V_s=600$  m/s) and rock ( $V_s=1000$  m/s) sites for the structure. The time history analysis is performed by applying three earthquakes, i.e., 1940 El Centro, 1989 Loma Prieta, and 1995 Kobe ground motions. Finally the wavelet analysis is applied to investigate and assess the effects of SSI on seismic response of structures.

### 6.1 Natural frequencies

Modal analysis has been applied to evaluate SSI effects on the fundamental period of NPP and BI-NPP structure rested on soft rock and rock site. Table 8 shows the change of the fundamental period of structures associated with SSI effect. As seen in Table 8 the first natural period (0.241 sec) of NPP structure with soft rock is 11% higher than the first natural period (0.218 sec) of fixed base structure. Similarly for rock site the period (0.224 sec) of structure is increased by 3%. The results conclude that due to consideration of soft rock site beneath NPP structure the rate of increase of fundamental period is higher (around 8%) than the rock site. For BI-NPP structure the first natural period is increased from 2.064 to 2.069 and 2.065 sec which is smaller than 1% when underlying soil profile is considered as soft rock and rock respectively. In conclusion SSI has significant effect to the increase of fundamental period of the NPP and BI-NPP structures rested on two rock sites and the increment of fundamental period of the NPP structure is noticeable than the BI-NPP structure when soil profile is considered as soft rock.

Table 8 First natural periods of nuclear power plant models

Analysis case	NPP			BI-NPP		
	Without SSI	Soft Rock site	Rock site	Without SSI	Soft Rock site	Rock site
First natural period (sec)	0.218	0.241	0.224	2.064	2.069	2.065

Table 9 Maximum lateral displacements of nuclear power plant models

Ground motion	Maximum lateral displacement (m)						
	Analysis case						
	NPP			BI-NPP			
	Without SSI	Soft Rock site	Rock site	Without SSI	Soft Rock site	Rock site	Rock site
	Top Node	Top Node	Top Node	Bottom Node	Top Node	Top Node	Top Node
El Centro	0.023	0.013	0.017	0.129	0.130	0.129	0.130
Loma Prieta	0.042	0.024	0.032	0.266	0.267	0.269	0.268
Kobe	0.036	0.043	0.043	0.201	0.202	0.203	0.203

### 6.2 Lateral displacement

The sensitivity of lateral displacements is investigated for both NPP and BI-NPP models considering effects of SSI. Table 9 demonstrates the effect of SSI on the lateral displacements of top node of the NPP and BI-NPP structure. It is observed from Table 9 that due to considering soft rock and rock site under NPP structure the top lateral displacement is reduced by 45.20% and 27.13% respectively for El Centro ground excitation and 43.2% and 25.04% respectively for Loma Prieta ground excitation. On the other hand under Kobe ground motion the top horizontal displacement of the structure is increased by around 17% for both rock sites. It is clear that for considering flexibility of NPP structure with soft rock under El Centro and Loma Prieta ground excitation the rate of decrease of top lateral displacement is greater (around 24%), while it is negligible under Kobe ground excitation. However, when flexibility is considered with soil profiles to BI-NPP structure the alteration of top lateral displacement is less than 1% under El Centro, Loma Prieta and Kobe ground excitations. The results conclude that, the effect of SSI on horizontal displacement of the BI-NPP structure is negligible for different ground motions, while for NPP structure the effect is prominent. Moreover the rate of fluctuation of horizontal displacement of NPP structure is more visible for soft rock site.

### 6.3 Total energy of acceleration response

Fig. 11 shows the profile of total accumulated energy for the applied records and responses of structures which characterizes the energy content through the duration of motions. It is obvious from Figs. 11 (a), (c), and (e) that total energy of the response of NPP provides highest value compared with the applied records. The maximum cumulative energy for El Centro record is  $11.2 \text{ m}^2/\text{s}^3$  which

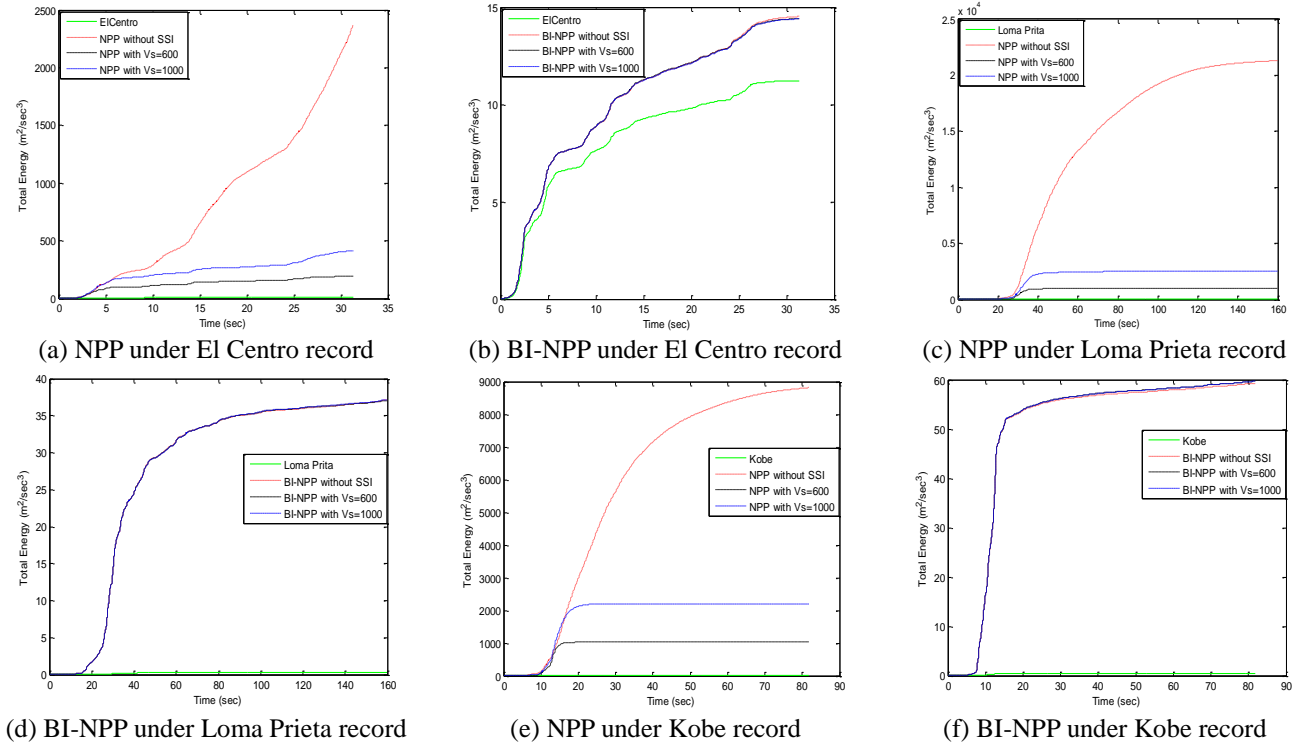


Fig. 11 Total energy profile of nuclear power plant models

is increased to  $2367.6 \text{ m}^2/\text{s}^3$  for the top response of NPP structure while for Loma Prieta and Kobe records it is raised from  $0.3 \text{ m}^2/\text{s}^3$  to  $21311.3 \text{ m}^2/\text{s}^3$  and  $0.5 \text{ m}^2/\text{s}^3$  to  $8817.2 \text{ m}^2/\text{s}^3$ , respectively. However, after considering SSI effect the energy associated with the response of NPP structure decreases dramatically. The maximum decrements are 92% and 83% for soft rock and rock sites under El Centro record, where the values are 95% and 88% for Loma Prieta and 88% and 75% for Kobe records due to considering two rock sites respectively. Furthermore, the decrease rate of total energy of response of structure is increased intensely which is more than 50% when flexibility is added with soft rock than the rock site. On the other hand, Figs. 11 (b), (d), and (f) illustrate that, the consideration of base isolation device to NPP significantly reduces the total energy of response of the structure. Figs. 11 (a) and (b) show that under El Centro excitation maximum energy of response of structure is dropped to  $14.5 \text{ m}^2/\text{s}^3$  from  $2367.6 \text{ m}^2/\text{s}^3$  when base isolators are installed. Similarly, the energy is decreased from  $21311.4 \text{ m}^2/\text{s}^3$  to  $37.1 \text{ m}^2/\text{s}^3$  and  $8817.2 \text{ m}^2/\text{s}^3$  to  $59.2 \text{ m}^2/\text{s}^3$  for Loma Prieta and Kobe records respectively. Moreover, it is evident from Figs. that, the consideration of SSI effect on base isolated NPP has negligible effect to change the total accumulated energy. The energy is reduced by 0.7% and 0.8% under El Centro and 0.2% and 0.1% under Loma Prieta records for incorporating flexibility with soft rock and rock sites respectively. However, for Kobe motion the energy is increased by 0.7% and 0.8% for two rock site conditions. It can be concluded that, the SSI effects have prominent role to minimize the energy content of acceleration response of NPP structure whereas the effects are unimportant for BI-NPP structure. Moreover, the decrease rate of total energy

of top response of NPP is increased dramatically when underlying soil is replaced by soft rock.

#### 6.4 Energy distribution at different levels

In Fig. 12, the energy distribution at different decomposition levels of applied ground motions and acceleration responses of structures are plotted with application of SSI. It is seen that El Centro, Loma Prieta, and Kobe ground motions are “broad-banded” records, which means that the energy ratios from the records are spread over a wide level of frequencies. Around 93% of the total energy of El Centro excitation is contained in levels 2-6 (i.e. between 0.39 and 12.5 Hz). Similarly, more than 90% energy belongs to the levels 4-8 and 3-7 for Loma Prieta and Kobe ground motions respectively. The fundamental frequencies of NPP models (with and without considering SSI effect) are determined from dynamic modal analysis and found to vary between 4.1 Hz to 4.6 Hz, which lie in level 3 corresponding to frequency range of 3.125 Hz to 6.25 Hz under El Centro record. Therefore, it is noticed from Fig. 12 (a) that the energy portion of response of structure in level 3 is increased from 28.2% to more than 80% than the applied ground motion. However, other higher frequency levels (4-7) of response signal has less than 10% of the total energy. Likely, for Loma Prieta and Kobe records the largest part of energy of response set to more than 80% has been concentrated in levels 5 and 4 respectively which contains the fundamental frequency of the structure shown in Figs. 12 (c) and (e). However, consideration of SSI to NPP display similar energy distributions to the response of structure. Under all ground excitations the change of energy contribution at different

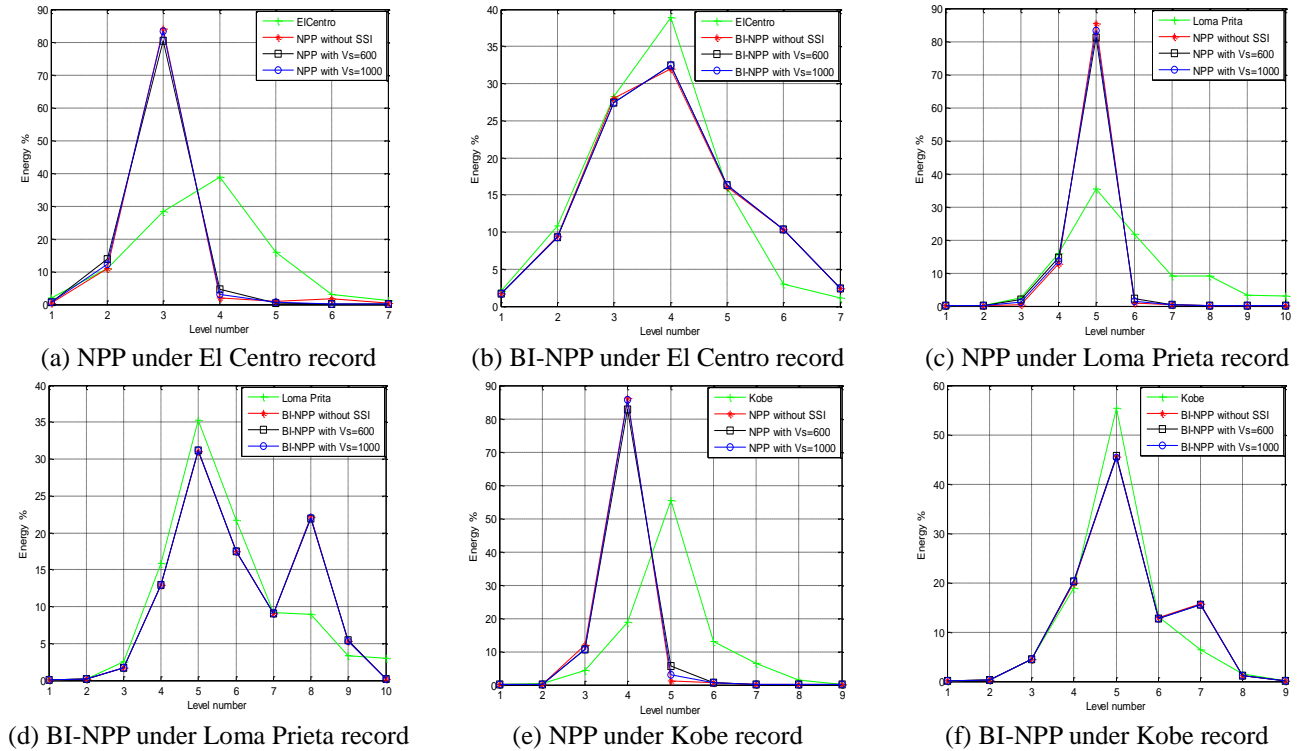


Fig. 12 Energy distribution at each decomposition level of nuclear power plant models

frequency levels due to SSI effect is less than 5%. These results indicate that, for NPP structure the energy distribution is dominated by natural frequency of structure and demands more high frequency content than the input ground motions, while, SSI has negligible effect to alter the energy distribution of each frequency level of the structure.

On the other hand, Figs. 12 (b), (d), and (f) show the response energy of structure is disseminated to the wide range of frequencies when flexibility to the base is adopting by installing base isolation device. The proportion of energy of response of BI-NPP is similar to that of applied ground records with the slightly higher ratios in level which contains the first natural frequency of structure. The energy ratio of El Centro record is increased from 3% to 10% in level 6 which holds fundamental frequency of BI-NPP. Similarly, it jumps from 9% to 22% in level 8 and 6% to 15% in level 7 under Loma Prieta and Kobe records respectively. However, after adding SSI effects the decrease of energy portion at each decomposition level is negligible which is less than 2% under three ground excitations. Therefore, it can be concluded that after incorporating base isolation to the NPP structure the response energy distributed across a wide band of frequencies, while the SSI has minimal influence to alter it.

### 6.5 Comparison of ground motion and structural response

Goggins *et al.* (2006) illustrated that short term changes in the frequency content of a signal can be detected by wavelet analysis. Any temporal variation in frequency content of response signal indicates the changes in the

dynamic characteristics of structure such as an initiation of stiffness degradation of the structural elements. The change of wavelet coefficients can be identified by correlating both the input ground motion and the acceleration response of structure for each frequency band. The correlation coefficient is expressed as

$$\rho_{xyj} = \frac{\sum_i w_{xj} w_{yj}}{\sqrt{\sum_i w_{xj}^2} \sqrt{\sum_i w_{yj}^2}} \quad (32)$$

where  $w_{xj}$  and  $w_{yj}$  denote the details of input ground motion and the acceleration response of structure at level  $j$ . The  $\rho = 0$  means no correlation, while  $\rho = \pm 1$  indicates that the perfect correlation exist between input ground motion and acceleration response.

Fig. 13 quantifies the correlation between the wavelet coefficients for the ground motions and the acceleration responses of NPP and BI-NPP structure with considering soil structure interaction. Figs. 13 (a), (c), and (e) illustrate that, poor correlation exists for most of the frequency contents (levels) for NPP under three earthquake records. The level 3 which holds the fundamental frequency of structure with highest energy content under El Centro record exhibits lower correlation is shown in Fig. 13 (a). From Figs. 13 (c) and (e) similar observation can be made at level 5 for Loma Prieta and 4 for Kobe excitation. After adopting flexibility with considering SSI effect to structure, the correlation coefficient increases for all most all frequency levels. It is also noticed that relatively better correlation exists when NPP rested on soft rock under all earthquake cases. Whereas Figs. 13 (b), (d), and (f) show good agreement between the ground and the top acceleration response wavelet coefficients of the BI-NPP

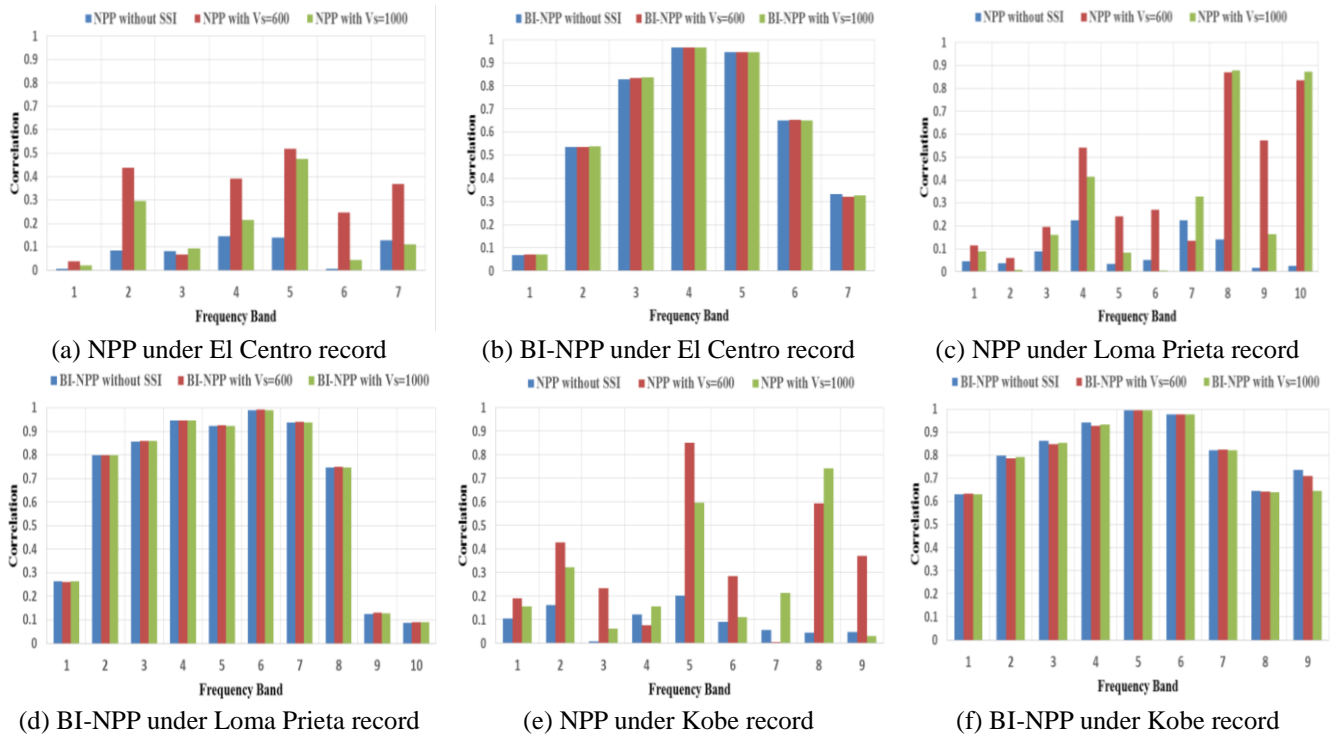


Fig. 13 Degree of correlation between ground motion and acceleration response of nuclear power plant models

structure. The levels 3-5 which contain most of the energy of acceleration response of structure, show nearly perfect correlation for El Centro ground excitation, as displayed in Fig. 13(b). Moreover, the level 6 holds fundamental frequency of BI-NPP structure, presents good relationship. Similarly Figs. 13 (d) and (e) show existence of good correlation at all frequency band which contain highest energy portions under Loma Prieta and Kobe excitations. Furthermore, there is no significant change is noticed in relation between input motion and acceleration response of BI-NPP when SSI effects are considered with two rock sites. In summary, the frequency content of the response of NPP is not related to the input ground motion, whereas soft rock site relatively increases the relation. However, BI-NPP response directly correlates with input ground motion and the relation does not change much when flexibility is considered with SSI.

## 7. Conclusions

The present study has investigated the influence of soil-structure interaction effects on the response of nuclear power plant structure supported on base isolation devices subjected to earthquake forces. To evaluate the SSI effects on the dynamic properties of the structure the viscoelastic cone model has been used. The analysis results show that the SSI has noteworthy influence on the seismic responses of NPP structure than the BI-NPP structure. The influence is more tangible on the fundamental period and maximum lateral displacement of the structure when flexibility of base is considered with soft rock. To grasp SSI effects on the acceleration response of nuclear power plant structure a

mathematical tool named wavelet transform is used which is convenient to estimate the total energy of acceleration time-history. The numerical analysis results depict that the total output energy of NPP structure considering SSI effect especially with soft rock site is decreased significantly rather than fixed base NPP. This indicates that, NPP structure suffers less acceleration and hence less vibration when the flexibility is adopted with soil profiles. Whereas, energy content of response of BI-NPP are not variable for different soil conditions. Moreover, distribution of energy at different decomposition levels of acceleration response of the structure is evaluated to identify the frequency range containing maximum portion of energy of the response. The observation shows that the response energy of NPP structure is concentrated around fundamental frequency, while it is disseminated to the wide range of frequencies and does not suffer much change due to SSI effect for BI-NPP structure. Furthermore, the correlation between ground motions and acceleration response of structures with SSI has been evaluated for detecting the short term changes in the frequency content which leads to identify the variations in the dynamic characteristics of the structure. The degree of correlation inversely proportional to the amount of resonance experienced a particular frequency band of acceleration response. The results show that SSI has noticeable influence in increase the relationship for NPP structure than BI-NPP structure. By summing up the findings of this study it can be concluded that wavelet analysis is an efficient tool to evaluate the effects of SSI on the seismic response of nuclear power plant structures. It also demonstrated that the consideration of SSI is important for NPP structure which shows beneficial effects to reduce the responses of structure and for BI-NPP structure the horizontal responses are not sensitive to the effects.

## Acknowledgments

This work was supported by the Korea Institute of Energy Technology Evaluation and Planning (KETEP) and the Ministry of Trade, Industry & Energy (MOTIE) of the Republic of Korea (No. 20171510101960).

## References

- Ahmadi, E., Khoshnoudian, F. and Hosseini, M. (2015), "Importance of soil material damping in seismic responses of soil-MDOF structure systems", *Soil. Found.*, **55**(1), 35-44.
- Chatterjee, P. and Basu, B. (2004), "Wavelet-based non-stationary seismic rocking response of flexibility supported tanks", *Earthq. Eng. Struct. Dyn.*, **33**, 157-181.
- Daubechies, I. (1992), *Ten Lectures on Wavelets*, Society for Industrial and Applied Mathematics, Philadelphia, PA, USA.
- Forni, M. (2011), "Seismic isolation of nuclear power plants", *Contribution to the "Italy in Japan 2011" Initiative Science, Technology and Innovation*, 1-8.
- Forni, M., Poggianti, A. and Dusi, A. (2012), "Seismic isolation of nuclear power plants", *Proceedings of the 15th World Conference of Earthquake Engineering*, paper no. 1485, Lisbon, Portugal, September.
- Ghaffar-Zade, M. and Cahpel, F. (1983), "Frequency-independent impedance of soil-structure system in horizontal and rocking modes", *Earthq. Eng. Struct. Dyn.*, **11**, 523-540.
- Goggins, J., Broderick, B.M., Basu, B. and Elghazouli, A.Y. (2006), "Investigation of the seismic response of braced frames using wavelet analysis", *Struct. Control Hlth. Monit.*, **14**, 627-648.
- Goupillaud, P., Grossmann, A. and Morlet, J. (1984), "Cycle-octave and related transforms in seismic signal analysis", *Geoexplorat.*, **23**(1), 85-102.
- Huang, Y.N., Whittaker, A.S. and Luco, N. (2010), "Seismic performance assessment of base-isolated safety-related nuclear structures", *Earthq. Eng. Struct. Dyn.*, **39**, 1421-1442.
- International Standard Organization (ISO) (2010), *Elastomeric Seismic-Protection Isolators-Part 3: Applications for Buildings-Specifications*, ISO 22762-3.
- Iyama, J. and Kuwamura, H. (1999), "Application of wavelets to analysis and simulation of earthquake motions", *Earthq. Eng. Struct. Dyn.*, **28**, 255-272.
- Kani, N., Takayama, M. and Wada, A. (2006), "Performance of seismically isolated buildings in Japan", *Proceedings of the 8th US national Conference of Earthquake Engineering*, Paper No. 2181, San Francisco, CA, USA, April.
- Kayen, R.E. and Mitchell, J.K. (1997), "Assessment of liquefaction potential during earthquakes by Arias intensity", *J. Geotech. Geo-environ. Eng.*, **128**(12), 1162-1174.
- Kenarangi, H. and Rofooei, F.R. (2010), "Application of tuned mass dampers in controlling the nonlinear behaviour of 3-D structural models, considering the soil-structure interaction", *Proceedings of the 5th National Congress on Civil Engineering*, Mashhad, Iran, May.
- Lee, N.H. and Song, K.B. (1999), "Seismic capacity evaluation of the prestressed/reinforced concrete containment, Young-Gwang nuclear power plant units 5 & 6", *Nucl. Eng. Des.*, **192**, 189-203.
- Li, H.N., He, X.Y. and Yi, T.H. (2009), "Multi-component seismic response analysis of offshore platform by wavelet energy principle", *Coast. Eng.*, **56**, 810-830.
- Mahmoud, S., Austrell, P. and Jankowski, R. (2012), "Simulation of the response of base-isolated buildings under earthquake excitations considering soil flexibility", *Earthq. Eng. Eng. Vib.*, **11**(3), 359-374.
- Malushte, S. and Wittaker, A.S. (2005), "Survey of past base isolation applications in nuclear power plants and challenges to industry/regulatory acceptance", *Proceedings of 18th International Conference on Structural Mechanics in Reactor Technology*, SMiRT 18, Beijing, China, August.
- Meek, J.W. and Wolf, J.P. (1993), "Cone models for nearly incompressible soil", *Earthq. Eng. Struct. Dyn.*, **22**(8), 649-663.
- Meek, J.W. and Wolf, J.P. (1993), "Why cone models can represent the elastic half-space", *Earthq. Eng. Struct. Dyn.*, **22**, 759-771.
- Melhem, H. and Kim, H. (2003), "Damage detection in concrete by Fourier and wavelet analysis", *J. Eng. Mech.*, ASCE, **129**(5), 571-577.
- Meyer, Y. (1992), *Wavelets and Operators*, Cambridge University Press, New York.
- Micheli, I., Cardini, S., Colaiuda, A. and Turrone, P. (2004), "Investigation upon the dynamic structural response of a nuclear plant on a seismic isolating devices", *Nucl. Eng. Des.*, **228**, 319-343.
- Newland, D.E. (1994), "Wavelet analysis of vibration, Part 1: Theory", *J. Vib. Acoust.*, ASME, **116**, 409-416.
- Newland, D.E. (1994), "Wavelet analysis of vibration, Part 2: Wavelet maps", *J. Vib. Acoust.*, ASME, **116**, 417-425.
- Novak, M. and Henderson, P. (1989), "Base-isolated buildings with soil-structure interaction", *Earthq. Eng. Struct. Dyn.*, **18**, 751-765.
- Sarica, R.Z. and Rahman, M.S. (2003), "A wavelet analysis of ground motion characteristics", *Proceedings of the U.S.-Taiwan workshop on soil liquefaction*, Taiwan.
- Schellenberg, A., Yang, T.Y. and Kohama, E. (2013), *OpenSees Navigator 2.5.2*, <https://nees.org/resources/osnavigator>.
- Sharmin, F., Hussan, M., Kim, D. and Cho, S.G. (2017), "Influence of soil-structure interaction on seismic responses of offshore wind turbine considering earthquake incident angle", *Earthq. Struct.*, **13**(1), 39-50.
- Spyrakos, C.C., Koutromanos, I.A. and Maniatakis, Ch.A. (2009), "Seismic response of base-isolated buildings including soil-structure interaction", *Soil Dyn. Earthq. Eng.*, **29**, 658-668.
- Stewart, J.P., Conte, J.P. and Aiken, I.D. (1999), "Observed behaviour of seismically isolated buildings", *J. Struct. Eng.*, ASCE, **125**(9), 955-964.
- Tongaonkar, N.P. and Jangid, R.S. (2003), "Seismic response of isolated bridges with soil-structure interaction", *Soil Dyn. Earthq. Eng.*, **23**(4), 287-302.
- Walker, J.S. (1999), *A Primer on Wavelets and Their Scientific Applications*, Chapman and Hall/CRC, New York.
- Wolf, J.P. (1994), *Foundation Vibration Analysis Using Simple Physical Models*, New Jersey, Prentice-Hall, Englewood Cliffs, NJ.
- Wong, H.L., Luco, J.E. and Trifunac, M.D. (1977), "Contact stresses and ground motion generated by soil-structure interaction", *Earthq. Eng. Struct. Dyn.*, **5**, 67-79.
- Yi, T.H., Li, H.N. and Gu, M. (2013), "Wavelet based multi-step filtering method for bridge health monitoring using GPS and accelerometer", *Smart Struct. Syst.*, **11**(4), 331-348.
- Zhao, C. and Chen, J. (2013), "Numerical simulation and investigation of the base isolated NPPC building under three-directional seismic loading", *J. Nucl. Eng. Des.*, **265**, 484-496.